LAND DEGRADATION & DEVELOPMENT
Land Degrad. Develop. (2017)
Published online in Wiley Online Library (wileyonlinelibrary.com) **DOI**: 10.1002/ldr.2665

VARIABILITY IN SOIL HYDRAULIC CONDUCTIVITY AND SOIL HYDROLOGICAL RESPONSE UNDER DIFFERENT LAND COVERS IN THE MOUNTAINOUS AREA OF THE HEIHE RIVER WATERSHED, NORTHWEST CHINA

Jie Tian[1], Baoqing Zhang[1]*, Chansheng He[1,2]*, Lixiao Yang[1]
[1]*Center for Dryland Water Resources Research and Watershed Science, Key Laboratory of West China's Environmental System (Ministry of Education), College of Earth and Environmental Sciences, Lanzhou University, Lanzhou, Gansu 730000, PR China*
[2]*Department of Geography, Western Michigan University, Kalamazoo, MI 49008, USA*

Received 5 July 2016; Revised 2 November 2016; Accepted 3 November 2016

ABSTRACT

Understanding the variability in soil hydraulic conductivity in the mountainous headwaters is critical to the modeling of mountainous runoff and the water resources management of river basins, especially in the arid and semiarid areas. In this study, a total of 32 soil profiles with five layers within 0–70 cm were sampled under different land cover types: forest, meadow, high coverage grassland (HCG), medium coverage grassland (MCG), and barren land in the upper stream of the Heihe river watershed, Northwest China. Saturated hydraulic conductivity (K_S) was measured for each sample. The vertical variation of K_S and soil hydrological response under different land covers were analyzed. Results show that K_S value in layer 5 was significantly lower than the values of above four layers. K_S decreased in the order of forest, meadow, HCG, MCG, and barren land, corresponding to the degree of vegetation degradation. The K_S decreased with depth under forest, HCG, and barren land, but increased first and then decreased under meadow and MCG. The dominant stormflow paths for different land covers were different: forest was dominated by deep percolation, HCG was dominated by subsurface flow (SSF), meadow was prevailed by Hortonian overland flow and had no SSF, while MCG and barren land were also dominated by Hortonian overland flow, but still formed SSF. This result provides important information for improving the accuracy of mountainous hydrological modeling and, in turn, leading to sustainable management of water resources in the study watershed. Copyright © 2016 John Wiley & Sons, Ltd.

KEY WORDS: saturated hydraulic conductivity; soil hydrological response; land cover; the Heihe river watershed; mountainous area

INTRODUCTION

Water is a key component of the earth system, and the quantity and quality of the water determines the land degradation (Eskandari *et al*., 2016; Giménez-Morera *et al*., 2010; Zhang & An, 2016). Mountainous areas are the water tower of the world for its importance in providing the freshwater supply for the downstream areas, and the mountainous areas have gained increasing attention recently in the context of climate change and adaptation (Viviroli *et al*., 2007; Immerzeel *et al*., 2010). Mountain runoff provides up to 95% of the freshwater supply in some catchments (Liniger *et al*., 1998; Zhang *et al*., 2016), particularly in arid and semi-arid areas (Chen *et al*., 2003). Thus, understanding the variability of the mountain runoff is vital to the sustainable management of water and land resources and welfare of people downstream in the arid and semi-arid areas. The accuracy of modeling of mountainous watershed hydrology is closely related to the accuracy of hydrological parameters, such as soil infiltrability and saturated hydraulic conductivity (K_S) (Zimmermann *et al*., 2006) and dynamics of hydrological processes in the Alpine area. K_S is one of the critical hydraulic factors that affect water movement and storage and energy exchange at the land surface (Lin, 2010; Jarvis *et al*., 2013; Vereecken *et al*., 2015); it is also one of the key input parameters in hydrological models (McDonnell & Beven, 2014; Ghimire *et al*., 2014; Jin *et al*., 2015). Thus, understanding the variation of the soil hydraulic properties such as K_S is crucial to both hydrological modeling and management of land degradation and development (Bonell *et al*., 2010; Ghimire *et al*., 2013; Gao *et al*., 2014).

The variability in soil hydraulic properties at large scale affects regional scale hydrological study (McDonnell & Beven, 2014; Jin *et al*., 2015). However, it is poorly understood because of the difficulties of conducting soil hydraulic property measurement in the high and cold mountainous area (Mcmillan & Srinivasan, 2015). At present, most studies focused on the horizontal variation of surface K_S at the small scale, including the variation of K_S at field scale (Rachman *et al*., 2004; Zimmermann & Elsenbeer, 2008; Gwenzi *et al*., 2011) and the hillslope scale (Wang *et al*., 2008; Chen *et al*., 2009; Archer *et al*., 2013; Ghimire *et al*., 2013; Liu *et al*., 2013). The vertical variation of K_S was studied based on limited profiles in small area (Blanco-Canqui *et al*., 2002; Coquet *et al*., 2005; Wang *et al*., 2013a; Branham & Strack, 2014; Schwen *et al*., 2014). Because of the high variability in soil hydraulic

*Correspondence to: B. Zhang and C. He, Key Laboratory of West China's Environmental System (Ministry of Education), College of Earth and Environmental Sciences, Lanzhou University, Lanzhou, Gansu 730000, PR China.
Emails: he@wmich.edu (C. He); baoqzhang@lzu.edu.cn (B. Zhang)

properties (Wang *et al*., 2012), it is difficult to apply the *in situ* observation result at small scale to the regional scale hydrological modeling (He & Croley, 2007; Brocca *et al*., 2012). Moreover, although remote sensing can provide spatial distribution of soil hydraulic properties in large area, it mainly focuses on the soil surface (depth < 5 cm), and its accuracy is still variable (Brocca *et al*., 2011). Because of the absence of *in situ* observed soil hydraulic parameters at regional scale, *in situ* profile measurements in large area are essential for improving the accuracy of hydrological simulations, which can also provide new insights in the spatial behavior of soil hydraulic properties at regional scale.

Land cover change has great influence on soil hydraulic properties (Gao *et al*., 2014; Zhao *et al*., 2014, 2015; Shi et al., 2015). Many studies have concluded that the surface K_S increased with the rehabilitation of degraded grassland to forest (Godsey & Elsenbeer, 2002; Li & Shao, 2006; Ilstedt *et al*., 2007; Zimmermann & Elsenbeer, 2008; Bonell *et al*., 2010; Price *et al*., 2010; Archer *et al*., 2013; Wang *et al*., 2013b). Studies also reported that K_S decreased with increasing depth along soil profiles (Blanco-Canqui *et al*., 2002; Schwen *et al*., 2014; Fu *et al*., 2015). Hwang *et al*. (2012) reported an exponential delay factor for variation of K_S along depth in the ecohydrological model (RHESSys) in North Carolina, USA. However, Coquet *et al*. (2005) found increasing of K_S with depth in two profiles in France, while Ghimire *et al*. (2013) found that K_S increased from surface to 0·25 m and then decreased from 0·25 to 1 m in a headwater catchment of Nepal. However, few studies have systematically compared dynamics of the vertical variation of K_S across different land cover types including barren land, grassland, meadow, and forest in the large mountainous watersheds.

Vertical variation of K_S, in combination with precipitation intensity, has been demonstrated to influence the dominant stormflow pathways (Chen *et al*., 2006; Zimmermann *et al*., 2006; Hellebrand *et al*., 2007; Bonell *et al*., 2010; Archer *et al*., 2013; Ghimire *et al*., 2013), including Hortonian overland flow (HOF, occurs when precipitation intensity exceeds the infiltration capability of surface soil horizon; Horton, 1933), saturated overland flow (surface flow due to the saturation of soil) or subsurface flow (SSF, lateral subsurface flow due to lateral flow structures), and deep percolation (DP, water percolated through the soil profile) (Scherrer & Naef, 2003; Ghimire *et al*., 2014). Researchers also reported how runoff process changed under different land cover types in the Alpine watersheds in Northwest China (He *et al*., 2012; Chen *et al*., 2014). However, little has been reported on how precipitation, K_S, and land cover types affected runoff pathways and soil hydrological responses in the mountainous watersheds.

This study aims to understand the variation of K_S and soil hydrological processes under different land cover types in a high elevation, topographically complex Alpine watershed, Northwest China, through *in situ* observations. The paper first describes the variation of K_S under different land covers and then analyzes the vertical variation of K_S with depth in soil profiles under different land covers. Finally, we discuss different runoff pathways and the soil hydrological responses under different land covers in the upper stream of the Heihe river watershed, Northwest China.

MATERIAL AND METHODS

Study area

This research was conducted in the upper stream of the Heihe river watershed, the second largest inland river watershed (or terminal lake) in China. It is located in Qilian Mountain, the northern margin of the Qinghai–Tibet Plateau, with an area of about 27×10^3 km^2 (97°29′-101°32′ E, 37°43′-39°39′ N) (Figure 1). The mountain runoff provides almost all of the water for the entire watershed, sustaining the population of about 1·2 million and farmland of $2{\cdot}4 \times 10^5$ hectares in the midstream, one of the major grain production regions in China (Chen *et al*., 2005; He *et al*., 2009; Li *et al*., 2015).

Annual precipitation ranges from over 200 mm in the steppe to 700 mm in the peak of the mountain (Li *et al*., 2009); the mean annual evaporation is about 700–2000 mm (Pan & Tian, 2001). Most of the study area is over 2000–5600 m above sea level (a.s.l.), belonging to the semi-humid forestry grassland climatic zone and cold-humid climate (Zhang *et al*., 2001; Wu *et al*., 2014). The vertical difference of hydrothermal condition leads to the formation of various natural land cover types: grassland (47%), barren land (21%), and forest (14%) (Feng *et al*., 2013). The main soil types are Alpine steppe soil, chestnut soil, and Alpine frost desert soil (Li *et al*., 2009), and the main textures of the soils are silt, silt loam, and sandy loam (USDA classification).

Field sampling

In order to analyze the impact of land cover on soil hydraulic property, we selected 32 representative soil locations (profiles) based on the spatial pattern and area of the vegetation. These 32 soil profiles contain the main land covers (forest, meadow, high coverage grassland (HCG), medium coverage grassland (MCG), and barren land) and scattered across the upper stream of the Heihe river watershed (Jin *et al*., 2015) (Figure 1). Because of the steep topography, and rough, even dangerous road conditions, the 32 profiles represented the best coverage of the spatial variability of vegetation in the study area given the physical and resource constraints.

The undisturbed soil samples were collected by the metal cylinder (with height and internal diameter of 5 cm) with a thin silicone grease layer applied on the internal wall of the cylinder to avoid the wall-effect (Fodor *et al*., 2011; Fu *et al*., 2015). At each sampling site, five layers were sampled (layer 1: 0–10 cm; layer 2: 10–20 cm; layer 3: 20–30 cm; layer 4: 30–50 cm; layer 5: 50–70 cm). The cylinder was slowly pushed vertically at the middle depth of each layer to collect the undisturbed soil core for each layer (layer 1: 2·5–7·5 cm; layer 2: 12·5–17·5 cm; layer 3: 22·5–27·5 cm; layer 4: 37·542·5 cm; layer 5: 57·5–62·5 cm). Three

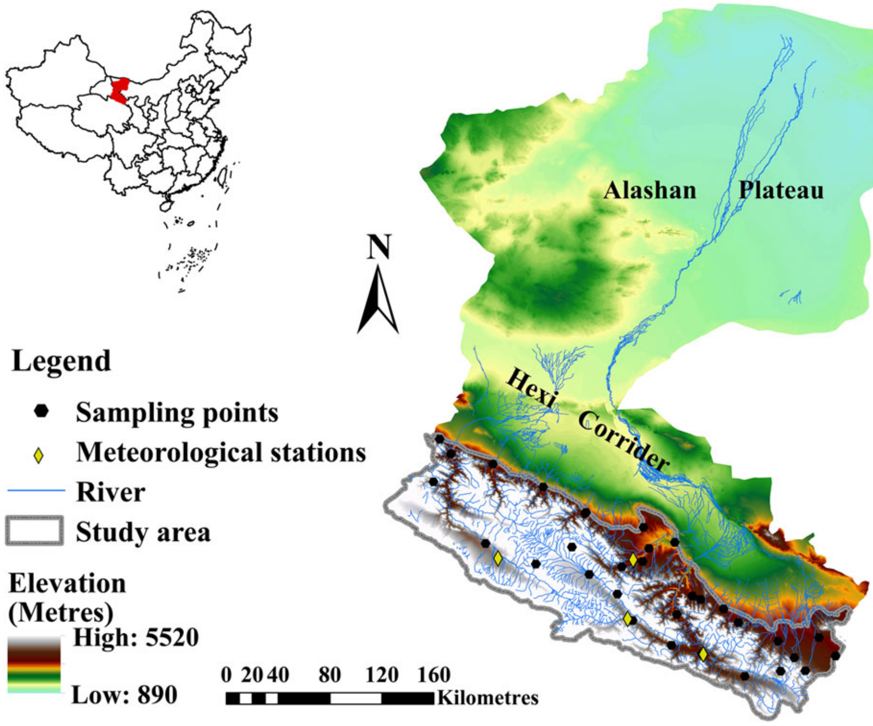

Figure 1. Study area and soil sampling/measurement locations in the upper stream of the Heihe river watershed, Northwest China. This figure is available in colour online at wileyonlinelibrary.com/journal/ldr

duplicate undisturbed samples were collected at each layer and taken to the laboratory to determine the K_S and soil bulk density. Meanwhile, the disturbed soil samples were also collected by the self-sealing bag after the collection of undisturbed sample at the same location for the analysis of soil organic matter and soil particle size distribution.

As one of the most spatially variable soil characteristics (Upchurch *et al*., 1988), K_s exhibits scale dependency (Lai & Ren, 2007; Bormann & Klaasen, 2008; Fodor et al., 2011) with regard to the volume of the measured soil. Although the small cylinder might underestimate K_S in the presence of macropore, it is still a widely used technique of collecting the undisturbed soil samples, especially in the high elevation, hard to reach Qilian mountain area (Lado *et al*., 2004; Benjamin *et al*., 2008; Gwenzi *et al*., 2011; Yao *et al*., 2013; Schwen *et al*., 2014; Shabtai *et al*., 2014; Fu *et al*., 2015; Yang *et al*., 2016). Facing with the physical and resource constraints in the topographically complex mountainous area, collecting the undisturbed soil samples in different layers with the small soil cores has been widely used and is more suitable to our regional scale study in the upper stream of the Heihe river watershed.

Other site-related parameters include the land cover type (forestland, meadow, high coverage grassland, medium coverage grassland, and barren land), soil type, and root depth for each soil profile. The 32 profiles were named from D1 to D32.

Among the collected 32 soil profiles, six profiles only had the first four layers, two profiles had three layers due to the fact that the depth of the study soil profiles only contained three to four layers, and the remaining had five layers. Thus, 150 soil samples were obtained and analyzed for the soil hydraulic and related properties in the laboratory.

Laboratory measurement of soil properties

The constant head method was used to measure K_S, which is based on the Darcy's law (Ilek & Kucza, 2014; Fu *et al*., 2015). Firstly, samples were saturated from the bottom in a container filled with water for 48 h. Then an empty cylinder with the same size was tightly secured to act as a reservoir, and the Mariotte bottle was used to keep a constant head to the core reservoirs. Lastly, the mass of water eluted from the sample cylinder was measured by an electronic balance in 5-min intervals until the flux rate became steady (the change of flux rate is less than 0·05 g at five consecutive readings) (Gwenzi *et al*., 2011). The experiment temperature (T, °C) was recorded using a thermometer. The saturated hydraulic conductivity at the experiment temperature ($K_{S,T}$) was calculated using Equation 1 and transformed to saturated hydraulic conductivity at 10 °C (K_S) using Equation 2 (Yi, 2009; Ilek & Kucza, 2014).

$$K_{S,T} = \frac{14.4 \times Q \times L}{A \times h \times t} \quad (1)$$

$$K_S = K_{S,T} \times \left(\frac{1.359}{1 + 0.0337 \times T + 0.00022 \times T^2} \right) \quad (2)$$

Where: 14·4 is a unit conversion factor that transfers the K_S from centimetres per minute to metres per day, $K_{S,T}$ is the saturated hydraulic conductivity at the measurement temperature T (m/d), Q is the percolated volume of water

(cm^3), L is the length of the soil column (5 cm), A is the cross-sectional area of the soil sample (19·6 cm^2), and h is the difference of hydraulic potential of soil column (h equals length of soil column plus height of water, 10 cm), t is the time interval (min). K_S is the saturated hydraulic conductivity at 10 °C (m/d).

After the measurement of K_S, the undisturbed soil samples were retained for the determination of soil bulk density. The soil samples were oven-dried at 105 °C for 24 h and weighted (m_1); the mass of the metal cylinder (m_2) and the total soil volume (98·17 cm^3) were used to calculate the dry soil bulk density ($\rho_b = (m_1 - m_2)/98.17$: g cm^{-3}) (Gwenzi *et al.*, 2011). Soil particle size was determined using the disturbed soil by the Mastersizer 2000 laser diffraction particle size analyzer (Malvern, Wang *et al.*, 2007a); the soil particles were classified as silt, clay, and sand. Then the soil textural classification was determined from the percentages of sand, silt, and clay by the soil textural triangle (Soil Survey Division Staff, 1993). The soil organic matter was measured using the total organic carbon analyzer (HT 1300, Analytik Jena AG).

Statistical analysis

Experiment data might contain outliers because of field sampling and measuring errors, and the outliers should be removed from the dataset before the analysis. If the suspect item x_p satisfies Equation 3, the item is the outlier according to the Grubbs test (Grubbs, 1950).

$$|x_p - \bar{x}| \geq \lambda_{(\alpha,n)} \cdot s \quad (3)$$

$\bar{x}$ is the arithmetic mean, s is the standard deviation, $\lambda_{(\alpha,n)}$ is the critical values of Grubbs test at $\alpha = 0{\cdot}01$ level, and n is the sample size.

Descriptive statistics about the maximum, minimum, mean, and coefficient of variation (CV) were performed for the soil properties. Result of the Kolmogorov–Smirnov test ($p < 0{\cdot}05$) indicated that the dataset of K_S was logarithmic normally distributed. K_S was transformed using $\log_{10}$ before further statistics analysis (Bonell *et al.*, 2010; Archer *et al.*, 2013). One-way analysis of variance (ANOVA) was used to test the difference in soil texture for the soil samples and to evaluate the difference in soil properties under different land covers. Two-way ANOVA was used to identify the influence of land cover and soil texture on K_S. If the results of ANOVA were significantly different at the $p < 0{\cdot}05$ level, mean comparison of K_S was tested by the Fisher's least significant difference. In order to identify the relationship between soil properties and K_S, correlation analysis was performed and considered significant at $p < 0{\cdot}05$ level. All the statistics, ANOVA, and correlation analysis were performed by the SPSS (version 18.0, IBM, Armonk, NY, USA).

Polynomial fitting of K_S along depth

The variation patterns of K_S with depth under different land covers were analyzed by the polynomial fitting method (Yao *et al.*, 2013) in the Origin (version 8.5, OriginLab, Hampton, MA, USA). The best fitting equation was chosen by the equation with the highest determination coefficient.

Calculation of rainfall intensity–duration–frequency curves

By superimposing maximum precipitation intensity I_{max} on K_S of different layers, the runoff pathways can be interpreted to reveal the percentage of HOF, SSF and DP in response to a rainfall event.(Zimmermann *et al.*, 2006; Hellebrand *et al.*, 2007; Bonell *et al.*, 2010; Archer *et al.*, 2013; Ghimire *et al.*, 2013)

In this work, intensity–duration–frequency (IDF) curve was calculated based on the precipitation data of over 20 years (1990–2009) from the meteorological stations (Qilian, Tuole, Yeniugou, and Sunan) in the upper stream of the Heihe river watershed (Figure 1). Firstly, maximum daily precipitation intensity for three specific return intervals (RIs: 1, 10, and 100 years) ($I_{1,p}$) was derived through the Log-Pearson Type III frequency curve based on the frequency calculation of the precipitation data. Secondly, the $I_{1,p}$ was used to calculate the maximum 24-hour precipitation intensity at specific RIs ($I_{24,p}$) by Equation 4. Lastly, the maximum precipitation at duration (t) from 0·1 to 48 h at three RIs ($I_{t,p}$) was calculated through Equations 5 and 6.

$$I_{24,p} = \eta \times I_{1,p} \quad (4)$$

$$When\ 1h \leq t \leq 24h \quad I_{t,p} = I_{24,p} \times 24^{(n_2-1)} \times t^{(1-n_2)} \quad (5)$$

$$When\ t < 1h \quad I_{t,p} = I_{24,p} \times 24^{(n_2-1)} \times t^{(1-n_1)} \quad (6)$$

Where: η is the ratio of $I_{24,p}$ and $I_{1,p}$ (equal to 1·15), n_1 and n_2 are the rainstorm parameters ($n_1 = 0{\cdot}66$, $n_2 = 0{\cdot}77$ in the Qilian Mountain according to Niu *et al.*, 2004 and Liang *et al.*, 2008). The IDF curve was derived by plotting the $I_{t,p}$ versus the duration t (logarithmic curve) (Koutsoyiannis *et al.*, 1998) (Figure 5).

RESULTS AND DISCUSSION

Textures of the 150 soil samples were silt loam (114, 76%), silt (19, 13%), and sandy loam (16, 11%). Distribution of the samples in the land covers were MCG (40%), HCG (25%), meadow (19%), forestland (8%), and barren land (8%). Particle size fractions did not significantly differ among the land covers (Table I), indicating that the collected soils had similar particle size fractions among the land covers. Furthermore, the result of two-way ANOVA for K_S under the interaction of land cover and soil texture indicated that the influence of land cover on K_S was more important compared with soil texture ($p < 0{\cdot}01$) (Table II). Results of the Grubbs test for K_S showed that there were six outliers among the 150 soil samples; those outliers were removed from the dataset before the statistics analysis.

Impact of land cover on soil properties

Results of statistical analysis for the soil physical, chemical, and hydraulic properties under different land covers are shown in Table III. The CV for silt (0·19), clay (0·21), and

Table I. Comparisons of mean soil sand, silt, and clay percentage (g 100 g^{-1}) among different land covers

Land cover (%)	Sand (50–2000 µm)	Silt (2–50 µm)	Clay (<2 µm)
Forest land (8)	24·06a	69·24a	6·69a
Meadow (19)	32·31a	61·25a	6·43a
HCG (25)	22·39a	70·59a	6·98a
MCG (40)	27·27a	65·74a	6·95a
Barren land (8)	31·74a	62·11a	6·16a

Different letter represents significant difference for soil particle fraction among different land covers at $p < 0.05$ (LSD) within each column

soil compaction (ρ_b) (0·24) were greater than 0·16 and less than 0·35, showing a relatively moderate variability, and CVs for sand (0·51), soil organic carbon (SOC) (0·97), and K_S (0·96) were greater than 0·36, showing a strong variability according to Wilding (1985), which indicates that the SOC and K_S had the high spatial variability and the soil texture had the least spatial variability.

The soil compaction (ρ_b), SOC, and K_S were significantly affected by land cover; the effects of land covers on ρ_b were in the order of forest < HCG < meadow < MCG < barren land and on SOC were in the order of forest > meadow > HCG > MCG > barren land (Table III). The different trends for SOC and ρ_b were due to the fact that better vegetation coverage had larger root system and more intense biological activity in the soil, the soil becoming looser and accumulating more soil organic matter. The correlation analysis between soil properties and K_S showed that K_S was positively correlated to the SOC ($r = 0{\cdot}075$) and sand percentage (0·09), negatively correlated with ρ_b (−0·13), silt (−0·09), and clay percentage (−0·004), and K_S did not correlate significantly with the soil properties. The correlation among ρ_b, SOC, and K_S may be the reason that K_S decreased in order of forest > meadow > HCG > MCG > barren land.

Impact of land cover on K_S

The variation of K_S with soil depth (Table IV) showed that K_S increased with depth (cm) at the average rate of 0·01 ($m \times d^{-1} \times cm^{-1}$) within 0–20 cm first and then decreased with depth at the average rate of 0·0056 within 20–70 cm; the variation of K_S may be related to the distribution of root (Wang *et al*., 2008). As the root could increase K_S, the average depth of root was concentrated in 10–20 cm in the area according to the field survey. CV of K_S was lowest in

Table II. The two-way ANOVA for K_S under the influence of soil texture and land cover

Factor	DF	Sum of Squares	*F* Value	Sig
Soil texture	2	0·146	0·880	—
Land cover	4	1·293	3·891	**
Interaction	8	1·137	1·710	—
Error	96	7·977	—	—
Total	110	11·468	—	—

**Significant effects at $p < 0{\cdot}01$; the result indicated that the influence of land cover on K_S is more important compared with soil texture.

Table III. Summary of statistics (maximum, minimum, average, and coefficient of variation) and ANOVA for the soil bulk density (ρ_b), soil organic carbon (SOC), soil texture (sand, silt, clay), and soil saturated hydraulic conductivity (K_S) among the land covers

	Forest land				HCG				Meadow				MCG				Barren land			
	Max	Min	Ave	CV	Max	Min	Ave	CV	Max	Min	Ave	CV	Max	Min	Ave	CV	Max	Min	Ave	CV
ρ_b *	1·39	0·5	0·98	0·3	1·68	0·52	1·07	0·23	1·54	0·7	1·12	0·21	1·94	0·85	1·32	0·21	1·85	1·01	1·37	0·16
SOC*	13·77	0·2	6·75	0·55	14·51	0·3	3·96	0·92	12·06	0·18	5·54	0·57	9·19	0·11	1·71	1·27	1·61	0·3	1·06	0·4
Sand	50·83	9·02	24·06	0·53	52·2	8·74	22·39	0·43	66·91	7·46	32·31	0·56	74·58	5·93	27·27	0·53	42·53	9·77	31·74	0·3
Silt	83·36	44·59	69·24	0·17	85·26	42·79	70·59	0·13	86·46	29·88	61·25	0·28	86·98	22·98	65·74	0·21	82·89	51·41	62·11	0·15
Clay	8·7	4·58	6·69	0·18	10·73	4·79	6·98	0·21	9·46	3·21	6·43	0·25	12·52	2·44	6·95	0·25	7·34	4·26	6·16	0·12
K_S **	1·43	0·25	0·77	0·49	1·111	0·035	0·299	0·866	1·557	0·019	0·429	0·874	1·429	0·003	0·290	0·895	0·697	0·025	0·211	1·098

*Significant effects at $p < 0{\cdot}05$,
**Significant effects at $p < 0{\cdot}01$; unit of ρ_b, SOC, soil texture, K_S are g cm^{-3}, g 100 g^{-1}, g 100 g^{-1}, m d^{-1}, respectively; *SD* is the standard deviation. Ave is average, and CV is coefficient of variation, CV = *SD*/*Ave*.

Table IV. Result of descriptive statistics (maximum, minimum, average and coefficient of variation, CV) and ANOVA for average K_S (m/d) in 5 layers of 32 profiles

Layer	Max	Min	Ave	CV
1	1·224	0·019	0·371*	0·780
2	1·557	0·003	0·471*	0·885
3	1·429	0·023	0·390*	0·901
4	1·443	0·019	0·382*	0·980
5	0·951	0·003	0·222*	1·241
Total	1·557	0·003	0·373	0·956

Layer 1: 0 ~ 10 cm; 2: 10 ~ 20 cm; 3: 20 ~ 30 cm; 4: 30 ~ 50 cm; 5: 50 ~ 70 cm; CV = *SD*/*Ave*, *SD* is the standard deviation.
*Significant differences among different layers at $p < 0·05$.

the surface and increased with depth, showing a negative correlation with the mean of *Ks* (Table IV).

Result of ANOVA for K_S at different layers showed that there was significant difference for K_S among different layers ($p < 0·01$). Multiple comparison analysis by Fisher's LSD indicated that only K_S in layer 5 was significantly lower than in the other four layers because of the compaction of soil in layer 5, while the K_S within the other four layers did not show significant differences (Table IV).

The impact of land cover on K_S is shown in Table III and Figure 2. The mean values of K_S for different land covers were in the order of forest > meadow > HCG > MCG > barren land, indicating that K_S corresponding to the degree of vegetation degradation. The mean values of CVs for different land covers were in the order of barren land > MCG > meadow > HCG > forest, indicating that the higher mean value of K_S had lower variability. The result was similar to the findings of other studies that K_S decreased with the vegetation degradation (Godsey & Elsenbeer, 2002; Li & Shao, 2006; Ilstedt *et al*., 2007; Bonell *et al*., 2010; Price *et al*., 2010; Ghimire *et al*., 2013).

Figure 2 shows that K_S of different land covers were different significantly in the first layer; the meadow and forest had minimum and maximum K_S among all the land cover types, respectively, while there were no significant differences among the paired comparison for the other land cover types. The order of K_S in layer 2 for different land covers was forest > meadow > HCG > MCG > barren land, and K_S was not significantly affected by land covers in layer 2.

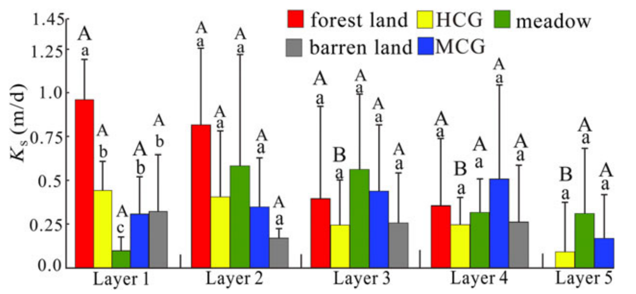

Figure 2. Vertical distribution of K_S in different layers. Different lowercase and capital letter show difference among land covers and layers, respectively ($p < 0.05$). K_S, saturated hydraulic conductivity; MCG, medium coverage grassland; HCG, high coverage grassland. This figure is available in colour online at wileyonlinelibrary.com/journal/ldr

The variation of K_S under different land covers in layers 3 to 5 was quite different from the first two layers. For example, for layers 3 and 4, the minimum values of K_S were all in HCG and the maximum values were in meadow and MCG, respectively, but the order for layer 5 was meadow > MCG > HCG. Thus, it appears that the K_S of soil below layer 1 was not controlled by the land cover overlying the profile. K_S of forest was always higher than that of barren land within 0–50 cm, and the root of forest was mainly distributed over 0–50 cm, indicating that the influence of land covers on K_S corresponds to the scope of root zone (Figure 2).

The results showed that the significant difference of K_S under different land covers only existed in layer 1 and the significant difference among different layers only existed in HCG (Figure 2). Ghimire *et al*. (2014) also concluded that the difference of K_S under different land covers was maximum at the depth of 0–10 cm.

Therefore, the impact of land cover on K_S mainly occurred at layer 1 (0–10 cm); land cover was not the major control factor for determining the spatial variation of K_S below layer 1.

Polynomial fitting of K_S with depth under different land covers

The polynomial fitting was used to analyze the distribution pattern of K_S with depth (Ibbitt & Woods, 2004; Hwang *et al*., 2012; Yao *et al*., 2013). Simple polynomial fitting (quadratic fitting and cubic fitting) and $\log_{10}$ transformed polynomial fitting (quadratic fitting and cubic fitting) were applied to all the 32 profiles, and the range of root zone was also plotted for each profile to explain the vertical variation of K_S (Figure 3). Additionally, an exponential fitting and log_{10} transformed exponential fitting were also fitted for the average vertical variation of K_S of different land cover types and the best fitting equations were selected (the highest coefficient of determination) for the five land cover types (Figure 4).

The influence of root on K_S was also analyzed by joining the range of root with distribution of K_S in soil profiles as the root can affect the hydraulic conductivity through the formation of macropores and system of continuous pores (Gyssels *et al*., 2005; Santra *et al*., 2008; Chen *et al*., 2009; Scholl *et al*., 2014) (Figure 3).

Figure 3 shows that the vertical distribution pattern of K_S for each profile was different among all 32 profiles, but the variation of K_S with depth was similar within the same type of land cover, the result was discussed as follows.

As shown in Figures 3 and 4, K_S decreased with depth at the average rate of 0·0198 ($m \times d^{-1} \times cm^{-1}$) for all profiles of forest, corresponding to the range of root distribution of forest (the range of root in the forest was >50 cm). The best fitting equation was quadratic fitting for the variation of K_S with depth in forest.

As can be seen in Figures 3 and 4, K_S increased with depth at the average rate of 0·024 from layer 1 to layer 2 and then decreased at the average rate of 0·01 for the

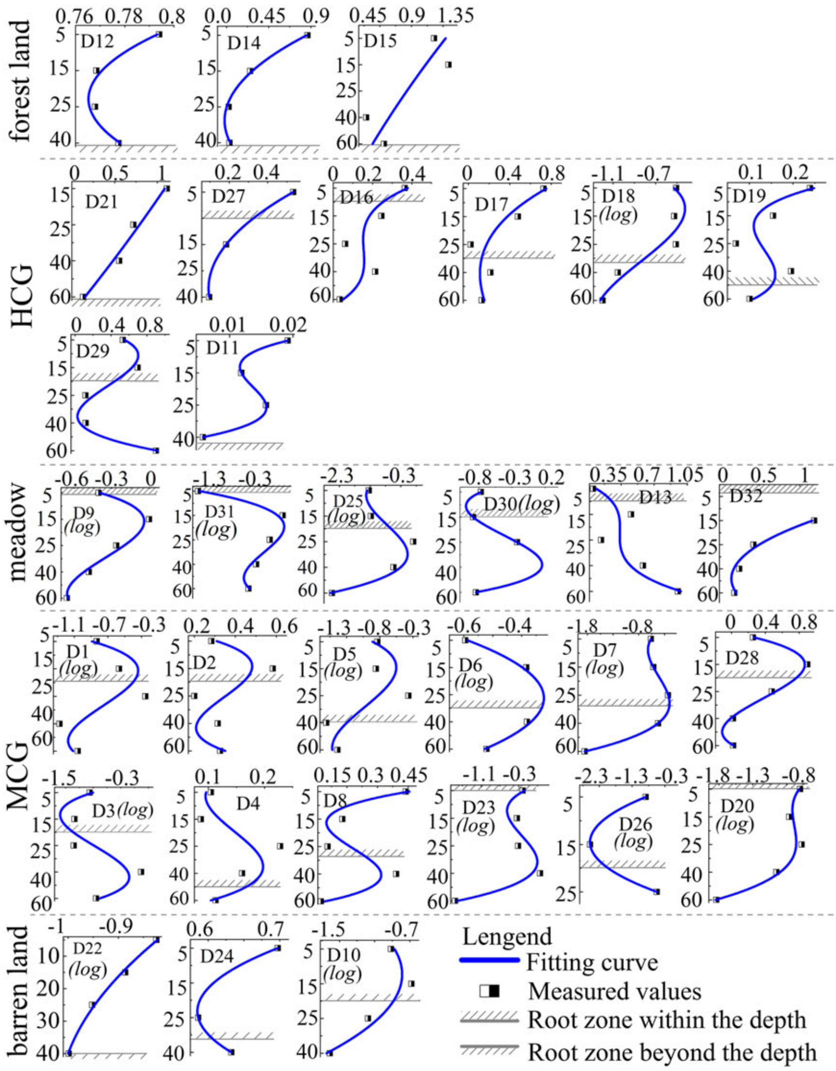

Figure 3. The fitting curve for the variation of K_S with depth for 32 profiles under different land covers and the depth of root for each profile (cm). The *x*-axis is the value of K_S or log(K_S) (m/d) (cm), and the *y*-axis is depth. (*log*) in each profile represents the curve fitted for log10 transformed K_S. K_S, saturated hydraulic conductivity; MCG, medium coverage grassland; HCG, high coverage grassland. D1 to D32 are the IDs of profiles for the soil sampling/measurement locations from 1 to 32. This figure is available in colour online at wileyonlinelibrary.com/journal/ldr

meadow, and the best fitting equation was $\log_{10}$ transformed cubic fitting.

K_S of the first layer under Alpine meadow was very low because of the influence of mattic epipedon of the Alpine meadow, which was formed by the abundant root system and its long-term interaction with the soil (Bao & Gao, 1994; Zeng *et al*., 2013); it can significantly influence the soil hydraulic property (Wang *et al*., 2007b).

Figures 3 and 4 show that the overall variation pattern of K_S under HCG was undulatory decreasing with depth, while the average K_S was steadily decreasing with depth at the rate of 0·0055 within 0–70 cm. The best fitting equation was quadratic fitting. As the average root zone was within 35 cm, it can be inferred that that the root of HCG can increase K_S.

The average variation of K_S along depth for MCG was increasing with depth from layers 1 to 4 at the rate of 0·0059 and then decreasing at the rate of 0·0017. The best fitting equation was cubic fitting (Figures 3 and 4).

The trend of K_S with depth in barren land was decreasing with depth at the rate of 0·0023 ($m \times d^{-1} \times cm^{-1}$). The best fitting equation was parabola model (Figures 3 and 4).

Soil hydrological processes under different land covers

K_S of different layers on the IDF curve for different land covers was plotted (Figure 5). Subsequently, soil hydrological processes and dominant stormflow pathways (DSP) during rainfall events were analyzed by comparing the precipitation intensity with vertical distribution of K_S, (Zimmermann *et al*., 2006; Hellebrand *et al*., 2007; Bonell *et al*., 2010; Ghimire *et al*., 2013).

We chose the maximum precipitation over 6 min ($I_{6max:}$ 26·4 mm h^{-1}) at 1-year return period as the index to infer the soil hydrological processes and DSPs under different land covers (Ghimire *et al*., 2013); the results are shown in Figure 6. The K_{S1}, K_{S2}, K_{S3}, K_{S4}, and K_{S5} were used to represent the K_S of layers 1, 2, 3, 4, and 5, respectively.

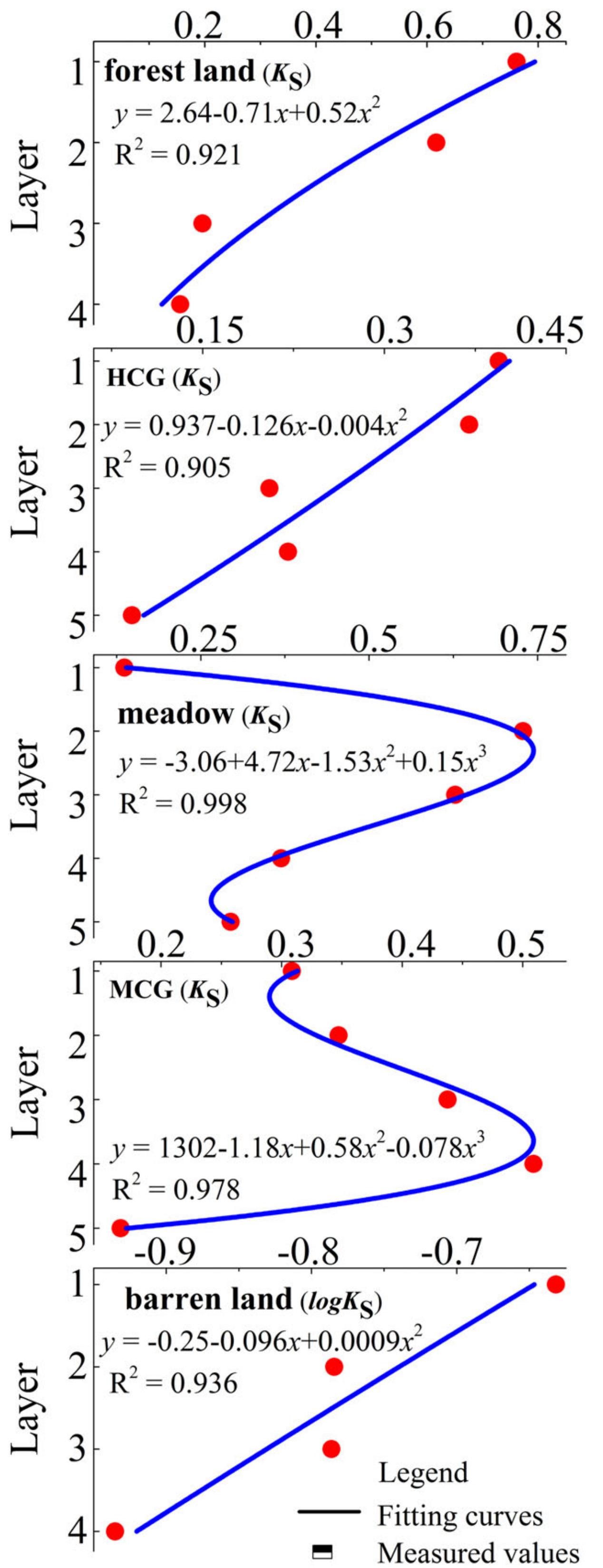

Figure 4. The best polynomial fitting for the variation of K_S with depth for the average values of different land covers. (KS) represents the equation fitted for the K_S, and (logK_S) means the equation fitted for log10 transformed K_S. The x-axis is the value of K_S or log(K_S) (m/d), and the y-axis is layer number. This figure is available in colour online at wileyonlinelibrary.com/journal/ldr

Forest

Figure 6a indicated that $K_{S1} > K_{S2} > I_{6max} > K_{S3} > K_{S4}$. Thus, the rainfall percolated through layers 1 and 2 (at the rate of 26·4 mm h^{-1}), and then water accumulated and formed a perched water-table or generated SSF on layers 3 (9·9 mm h^{-1}) and 4 (1·7 mm h^{-1}); finally, water vertically percolated through the soil profile at the rate of the minimum among the K_S of different layers and I_{6max} (14·8 mm h^{-1}). Our finding is similar with the conclusions of others that forest with high hydraulic conductivity could reduce the occurrence of Hortonian infiltration excess overland flow and increase the volume of precipitation recharging to deep soil compared with degraded grass (Zimmermann & Elsenbeer, 2009; Bonell *et al*., 2010; Ghimire *et al*., 2013; Archer *et al*., 2013).

HCG

As shown in Figure 6b, $I_{6max} > K_{S1} > K_{S2} > K_{S4} > K_{S3} > K_{S5}$. Thus, the rainfall ponded or generated HOF on the ground surface (10 mm h^{-1}) and percolated through layer 1 as the rate of K_{S1} (16·4 mm h^{-1}). Then water accumulated or generated SSF on layers 2 (1 mm h^{-1}) and 3 (6·8 mm h^{-1}); subsequently, water percolated through layers 2 to 4 and eventually accumulated or generated SSF on layer 5 (4·8 mm h^{-1}).

Meadow

Figure 6c manifested that K_S of layer 1 was the minimum among the five layers and I_{6max} was higher than K_{S1}. Therefore, the rainfall ponded or generated HOF on the ground surface (20·7 mm h^{-1}) and percolated through the whole soil profile at the rate of 5·7 mm h^{-1}.

MCG

Figure 6d indicated that $I_{6max} > K_{S4} > K_{S3} > K_{S2} > K_{S1} > K_{S5}$. Consequently, the rainfall ponded or generated HOF on the ground surface (13·5 mm h^{-1}), and then the water percolated through layers 1 to 4 at the rate of 12·9 mm h^{-1}. Even though part of water accumulated or generated SSF on layer 5 (6 mm h^{-1}), plenty of water still percolated through layer 5 (6·9 mm h^{-1}).

Barren land

Figure 6e demonstrated that $I_{6max} > K_{S1} > K_{S2} > K_{S3} > K_{S4}$. Hence, rainfall ponded or generated HOF on the ground surface (13 mm h^{-1}), and water accumulated or generated SSF on layers 2 (0·1 mm h^{-1}), 3 (2·7 mm h^{-1}), and 4 (0·1 mm h^{-1}), respectively. A fraction of water percolated through layer 4 (10·5 mm h^{-1}).

I_{6max} at 100-year RI: For the condition of I_{6max} at other recurrence intervals, the movement of water in soil could be inferred similarly as discussed previously. Taken forest land under 100-year RI as an example, Figure 6f manifested that $I_{6max} > K_{S1} > K_{S2} > K_{S3} > K_{S4}$, which had a parallel result to barren land as shown in Figure 6e. Consequently, rainfall ponded or generated HOF on the ground surface (73·9 mm h^{-1}); later, water accumulated or generated SSF

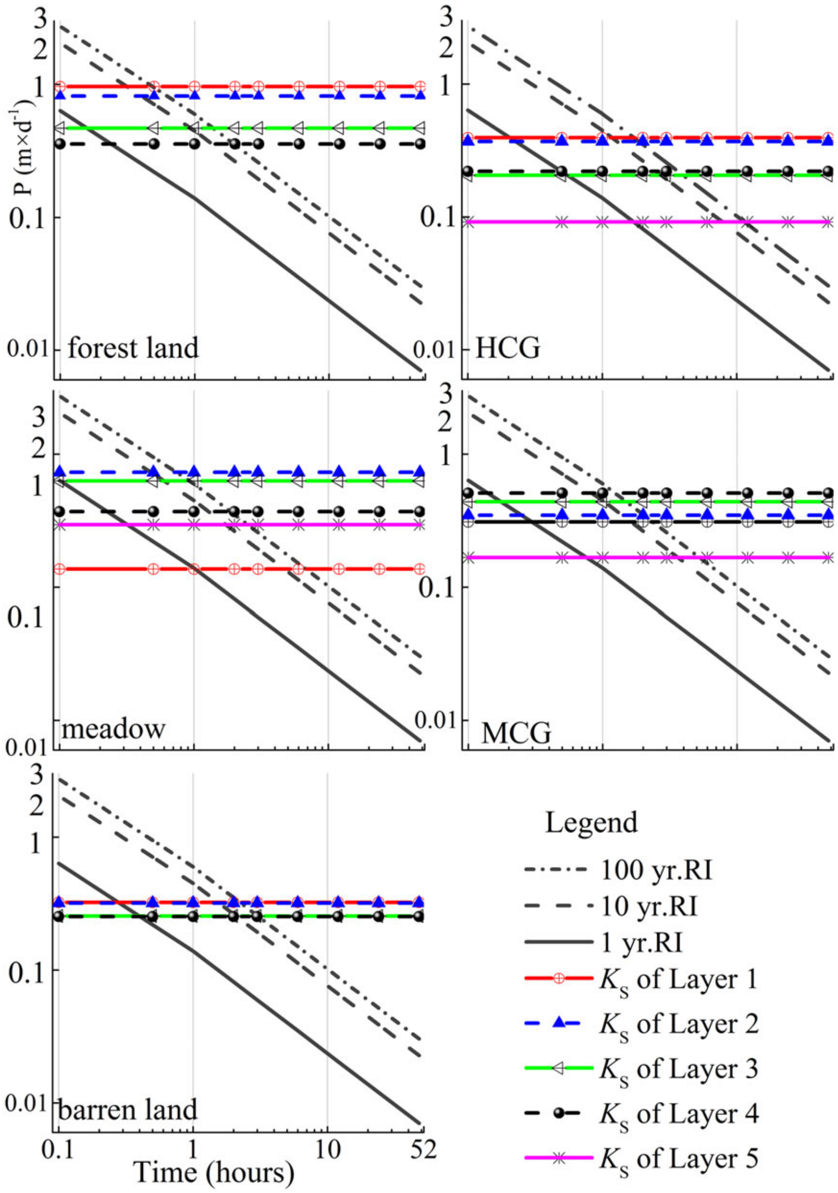

Figure 5. The calculated rainfall intensity/duration/frequency (IDF) curves aggregating rainfalls over 0·1–48-h durations for 1, 10, 100-year return periods (1 yr. RI, 10 yr. RI, 100 yr. RI) and the K_S of different layers for different land covers. *X*-axis is the duration time (*t*/hour), *y*-axis is the rainfall intensity (P), and K_S (m/d), MCG is medium coverage grassland, and HCG is high coverage grassland. This figure is available in colour online at wileyonlinelibrary.com/journal/ldr

on layers 2 ($6\,\mathrm{mm\,h^{-1}}$), 3 ($17{\cdot}5\,\mathrm{mm\,h^{-1}}$), and 4 ($1{\cdot}7\,\mathrm{mm\,h^{-1}}$), respectively. A fraction of water percolated through layer 4 ($14{\cdot}8\,\mathrm{mm\,h^{-1}}$).

Percentage of dominant stormflow path: The percentage of stormflow path under different land covers during or shortly after the rainfall event was calculated by dividing the rate of stormflow path by the precipitation intensity (Figure 6). For $I_{6\max}$ at 1-year RI, HOF mainly generated under meadow (78%), MCG (51%), barren land (49%), and HCG (38%), while forest land could not generate HOF; in addition, SSF was mainly emerged in HCG (48%), forest land (44%), MCG (23%), and barren land (11%), while no SSF for meadow; unlike other DSPs, DP was generated in all of the land cover types and increased in the order of HCG (14%), meadow (22%), MCG (26%), barren land (40%), and forest (56%) (Figure 6).

Hao and Zong (2013) reported that the forest land decreased before 2000 and increased after that in the upper stream of the Heihe river watershed; our result indicates that the increase of forest land is likely to increase the deep percolation and baseflow and vice versa; this was verified by the observations of Dang *et al*. (2011) and Zhang *et al*. (2011), while Yin *et al*. (2014) also confirmed the process by the simulation of SWAT in the upper stream of the Heihe river watershed.

In summary, under the $I_{6\max}$ at 1-year RI, the DSPs for different land covers were different. For the forest, the DSP was DP and rainfall percolated through layers 1 and 3

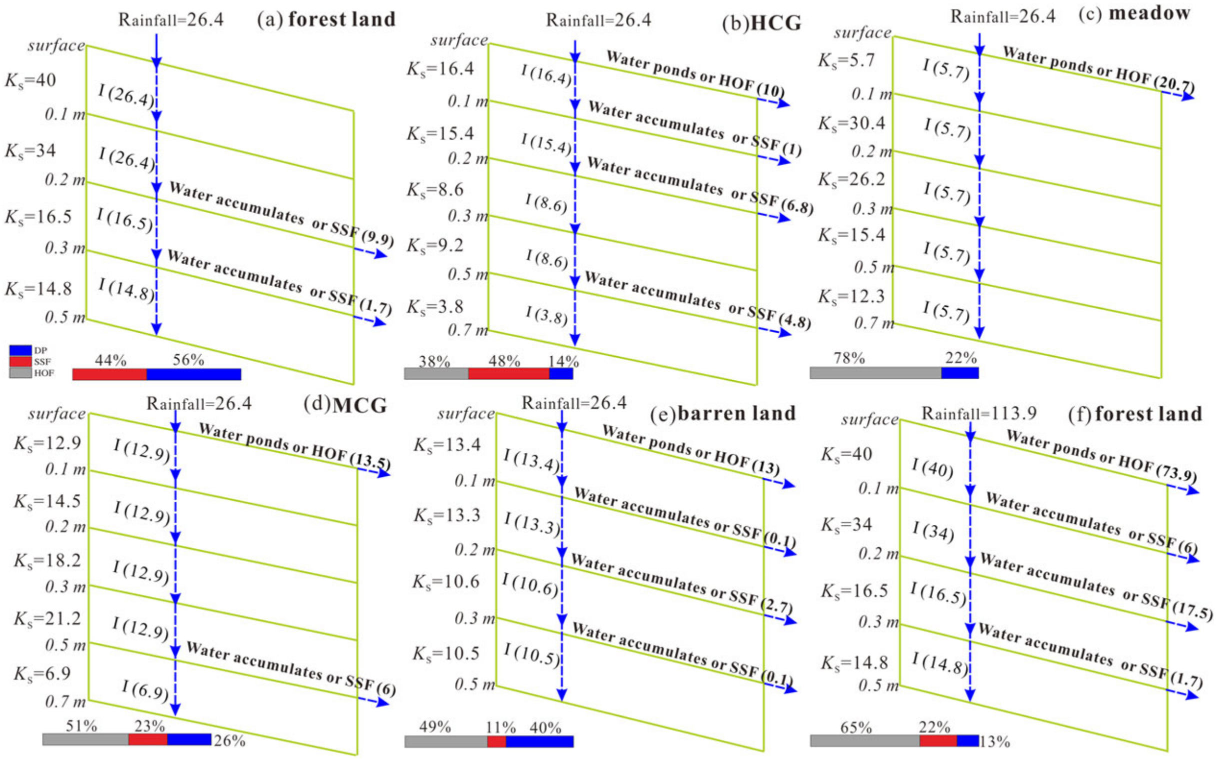

Figure 6. The percolation of rainfall at the rates of *I*6max of 26·4 mm h^{-1} (1-year return period: a, b, c, d, e) and 113·9 mm h^{-1} (100-year return period: f) through various soil layers for different land covers in the upper stream of the Heihe river watershed. The histogram is the representation for the percentage of different stormflow paths under different land covers. HOF is Horton overland flow, SSF is subsurface flow, DP is deep percolation, and the numbers in the parenthesis are the rate of the corresponding flows. Infiltration occurred in the whole soil profile and is abbreviated as *I*, and the numbers in the parenthesis are the infiltration rates. MCG is medium coverage grassland, and HCG is high coverage grassland. Unit of precipitation intensity, K_S and the rate of hydrological processes are mm h^{-1}. This figure is available in colour online at wileyonlinelibrary.com/journal/ldr

and generated SSF on layers 3 and 4. For the HCG, the DSP was SSF, the rainfall ponded or generated HOF on the surface ground, and SSF formed on the layers 2, 3, and 5. In the case of meadow, with the influence of mattic epipedon, the DSP was HOF generated on layer 1, and then water infiltrated through the profile. For the MCG, the DSP was HOF generated on layer 1 and, subsequently, rainfall percolated through layers 2–4 and generated SSF on layer 5. For barren land, the DSP was HOF generated on layer 1 and SSF was formed on layers 2, 3, and 4, respectively. The differences in runoff generation process under different land cover types must be taken into consideration in modeling of mountainous watershed hydrology.

CONCLUSIONS

We analyzed the vertical variation of hydraulic conductivity and identified the dominant stormflow paths under different land cover types in the upper stream of the Heihe river watershed. The main findings are as follows: (i) the spatial variation of K_S in the first layer (0–10 cm) was mainly controlled by land cover types, and K_S below 10 cm was not controlled by land cover in the study area; and (ii) K_S decreased in the order of forest, meadow, HCG, MCG, and barren land. The vertical variation pattern of K_S varied under different land covers: For the forest, HCG and barren land, K_S decreased along the profile; for meadow and MCG, it increased first and then decreased. The result reflects the influence of root on K_S; the polynomial fitting equation for the variation of K_S with depth under forest and barren land were quadratic model and for other land cover types were the cubic model; and (iii) the response of soil hydrological process and the dominant stormflow paths to precipitation under different land covers were different. For the forest, most of the water vertically percolated through the soil profile; and HCG was dominated by SSF; however, meadow was prevailed by HOF and had no SSF, while MCG and barren land were also dominated by HOF, but still formed SSF. These different hydrological responses must be taken into consideration in the future eco-hydrological modeling of the mountainous watersheds.

ACKNOWLEDGEMENTS

The project is partially funded by the National Natural Science Foundation of China (Grants: 91125010 and 41530752) and Scherer Endowment Fund of Department of Geography, Western Michigan University. We are grateful to the members of Center for Dryland Water Resources Research and Watershed Science, Lanzhou University for their hard field work to collect and analyze the soil data in the high and cold, hard to reach mountainous area.

REFERENCES

Archer NAL, Bonell M, Coles N, Macdonald AM, Auton CA, Stevenson R. 2013. Soil characteristics and landcover relationships on soil hydraulic conductivity at a hillslope scale: a view towards local flood management. *Journal of Hydrology* **497**: 208–222. DOI:10.1016/j.jhydrol.2013.05.043.

Bao XK, Gao YX. 1994. Recent treatises on Chinese soil taxonomic classification. Science press, Beijing, China: 302–309 (in Chinese).

Benjamin JG, Mikha MM, Vigil MF. 2008. Organic carbon effects on soil physical and hydraulic properties in a semiarid climate. *Soil Science Society of America Journal* **72**: 1357–1362. DOI:10.2136/sssaj2007.0389.

Blanco-Canqui H, Gantzer CJ, Anderson SH, Alberts EE, Ghidey F. 2002. Saturated hydraulic conductivity and its impact on simulated runoff for claypan soils. *Soil Science Society of America Journal* **66**: 1596–1602. DOI:10.2136/sssaj2002.1596.

Bormann H, Klaasen K. 2008. Seasonal and land use dependent variability of soil hydraulic and soil hydrological properties of two Northern German soils. *Geoderma* **145**: 295–302. DOI:10.1016/j.geoderma.2008.03.017.

Bonell M, Purandara B, Venkatesh B, Krishnaswamy J, Acharya H, Singh U, Jayakumar R, Chappell N. 2010. The impact of forest use and reforestation on soil hydraulic conductivity in the Western Ghats of India: implications for surface and sub-surface hydrology. *Journal of Hydrology* **391**: 47–62. DOI:10.1016/j.jhydrol.2010.07.004.

Branham JE, Strack M. 2014. Saturated hydraulic conductivity in Sphagnum – dominated peatlands: do microforms matter? *Hydrological Processes* **28**: 4352–4362. DOI:10.1002/hyp.10228.

Brocca L, Hasenauer S, Lacava T, Melone F, Moramarco T, Wagner W, Dorigo W, Matgen P, Martínez-Fernández J, Llorens P. 2011. Soil moisture estimation through ASCAT and AMSR-E sensors: an intercomparison and validation study across Europe. *Remote Sensing of Environment* **115**: 3390–3408. DOI:10.1016/j.rse.2011.08.003.

Brocca L, Tullo T, Melone F, Moramarco T, Morbidelli R. 2012. Catchment scale soil moisture spatial–temporal variability. *Journal of Hydrology* **422-423**: 63–75. DOI:10.1016/j.jhydrol.2011.12.039.

Chen RS, Kang ES, Lv SH, Ji XB, Yang Y, Zhang JS. 2006. A distributed water-heat coupled (DWHC) model for mountainous watershed of an inland river basin(II): model results using the measured data at the meteorological and hydrological stations. *Advances in Earth Science* **21**: 819–829. DOI:10.3321/j.issn:1001-8166.2006.08.006(in Chinese, with English Abstract).

Chen RS, Kang ES, Yang JP, Zhang JS. 2003. A distributed daily runoff model of inland river mountainous basin. *Advance In Earth Sciences* **13**: 198–206. DOI:10.3321/j.issn:1001-8166.2003.02.008(in Chinese, with English Abstract).

Chen RS, Yang Y, Han CT, Liu JF, Kang ES, Song YX, Liu ZW. 2014. Field experimental research on hydrological function over several typical underlying surfaces in the cold regions of Western China. *Advances in Earth Science* **29**: 507–514. DOI:10.11867/j.issn.1001-8166.2014.04.0507(in Chinese, with English Abstract).

Chen X, Zhang ZC, Chen XH, Shi P. 2009. The impact of land use and land cover changes on soil moisture and hydraulic conductivity along the Karst hillslopes of Southwest China. *Environmental Earth Sciences* **59**: 811–820. DOI:10.1007/s12665-009-0077-6.

Chen Y, Zhang DQ, Sun YB, Liu X, Wang NZ, Savenije HHG. 2005. Water demand management: a case study of the Heihe River Basin in China. *Physics\s&\schemistry of the Earth. Parts A/b/c* **30**: 408–419. DOI:10.1016/j.pce.2005.06.019.

Coquet Y, Vachier P, Labat C. 2005. Vertical variation of near-saturated hydraulic conductivity in three soil profiles. *Geoderma* **126**: 181–191. DOI:10.1016/j.geoderma.2004.09.014.

Dang SZ, Wang ZG, Liu CM. 2011. Baseflow separation and its characteristics in the upper reaches of the Heihe River Basin. *Resources Science* **33**: 2232–2237(in Chinese, with English Abstract).

Eskandari H, Borji M, Khosravi H, Mesbahzadeh T. 2016. Desertification of forest, range and desert in Tehran province, affected by climate change. *Solid Earth* **7**: 905–915. DOI:10.5194/se-7-905-2016.

Feng Q, Su YH, Si JH, Chang ZQ, Guo R HX, Chen LJ, Huo H, Qin YY. 2013. Ecohydrological transect survey of Heihe River Basin. *Advances in Earth Science* **28**: 187–196(in Chinese, with English Abstract).

Fodor N, Sándor R, Orfanus T, Lichner L, Rajkai K. 2011. Evaluation method dependency of measured saturated hydraulic conductivity. *Geoderma* **165**: 60–68. DOI:10.1016/j.geoderma.2011.07.004.

Fu TG, Chen HS, Zhang W, Nie YP, Wang KL. 2015. Vertical distribution of soil saturated hydraulic conductivity and its influencing factors in a small karst catchment in Southwest China. *Environmental monitoring and assessment* **187**: 1–13. DOI:10.1007/s10661-015-4320-1.

Gao XD, Wu PT, Zhao XN, Wang J, Shi YG. 2014. Effects of land use on soil moisture variations in a semi-arid catchment: implications for land and agricultural water management. *Land Degradation & Development* **25**: 163–172. DOI:10.1002/ldr.1156.

Ghimire CP, Bonell M, Bruijnzeel LA, Coles NA, Lubczynski MW. 2013. Reforesting severely degraded grassland in the Lesser Himalaya of Nepal: effects on soil hydraulic conductivity and overland flow production. *Journal of Geophysical Research Earth Surface* **118**: 2528–2545. DOI:10.1002/2013JF002888.

Ghimire CP, Bruijnzeel LA, Bonell M, Coles N, Lubczynski MW, Gilmour DA. 2014. The effects of sustained forest use on hillslope soil hydraulic conductivity in the Middle Mountains of Central Nepal. *Ecohydrology* **7**: 478–495. DOI:10.1002/eco.1367.

Giménez-Morera A, Ruiz Sinoga JD, Cerdà A. 2010. The impact of cotton geotextiles on Soil and water losses from Mediterranean rainfed agricultural land. *Land Degradation and Development* **21**: 210–217. DOI:10.1002/ldr.971.

Godsey S, Elsenbeer H. 2002. The soil hydrologic response to forest regrowth: a case study from southwestern Amazonia. *Hydrological Processes* **16**: 1519–1522. DOI:10.1002/hyp.605.

Grubbs FE. 1950. Sample criteria for testing outlying observations. *The Annals of Mathematical Statistics* **21**: 27–58. DOI:10.1214/aoms/1177729885.

Gwenzi W, Hinz C, Holmes K, Phillips IR, Mullins IJ. 2011. Field-scale spatial variability of saturated hydraulic conductivity on a recently constructed artificial ecosystem. *Geoderma* **166**: 43–56. DOI:10.1016/j.geoderma.2011.06.010.

Gyssels G, Poesen J, Bochet E, Li Y. 2005. Impact of plant roots on the resistance of soils to erosion by water: a review. *Progress in Physical Geography* **29**: 189–217. DOI:10.1191/0309133305pp443ra.

Hao ZC, Zong B. 2013. Land use and land cover change analysis in the upper reaches of the Heihe river. *China Rural Water and Hydropower* **10**: 115–118. DOI:10.3969/j.issn.1007-2284.2013.10.033(in Chinese, with English Abstract).

He CS, Demarchi C, Croleyii TE, Feng Q, Hunter T. 2009. Hydrologic modeling of the Heihe watershed by DLBRM in Northwest China. *Journal of Glaciology and Geocryology* **31**: 410–421.

He C, Croley TE, II. 2007. Application of a distributed large basin runoff model in the great lakes basin. *Control Engineering Practice* **15**: 1001–1011. DOI:10.1016/j.conengprac.2007.01.011.

He ZB, Zhao W, Liu H, Tang ZX. 2012. Effect of forest on annual water yield in the mountains of an arid inland river basin: a case study in the Pailugou catchment on northwestern China's Qilian Mountains. *Hydrological Processes* **26**: 613–621. DOI:10.1002/hyp.8162.

Hellebrand H, Hoffmann L, Juilleret J, Pfister L. 2007. Assessing winter storm flow generation by means of permeability of the lithology and dominating runoff production processes. *Hydrology and Earth System Sciences* **11**: 1673–1682. DOI:10.5194/hess-11-1673-2007.

Horton RE. 1933. The rôle of infiltration in the hydrologic cycle. *Eos, Transactions American Geophysical Union* **14**: 446–460. DOI:10.1029/TR014i001p00446.

Hwang T, Band LE, Vose JM, Tague C. 2012. Ecosystem processes at the watershed scale: hydrologic vegetation gradient as an indicator for lateral hydrologic connectivity of headwater catchments. *Water Resources Research* **48**: 109–119. DOI:10.1029/2011wr011301.

Ibbitt R, Woods R. 2004. Re-scaling the topographic index to improve the representation of physical processes in catchment models. *Journal of Hydrology* **293**: 205–218. DOI:10.1016/j.jhydrol.2004.01.016.

Ilek A, Kucza J. 2014. A laboratory method to determine the hydraulic conductivity of mountain forest soils using undisturbed soil samples. *Journal of Hydrology* **519**: 1649–1659. DOI:10.1016/j.jhydrol.2014.09.045.

Ilstedt U, Malmer A, Verbeeten E, Murdiyarso D. 2007. The effect of afforestation on water infiltration in the tropics: a systematic review and meta-analysis. *Forest Ecology and Management* **251**: 45–51. DOI:10.1016/j.foreco.2007.06.014.

Immerzeel WW, Van Beek LP, Bierkens MF. 2010. Climate change will affect the Asian water towers. *Science* **328**: 1382–1385. DOI:10.1126/science.1183188.

Jarvis N, Koestel J, Messing I, Moeys J, Lindahl A. 2013. Influence of soil, land use and climatic factors on the hydraulic conductivity of soil.

Hydrology and Earth System Sciences **17**: 5185–5195. DOI:10.5194/hess-17-5185-2013.
Jin X, Zhang LH, Gu J, Zhao C, Tian J, He CS. 2015. Modeling the impacts of spatial heterogeneity in soil hydraulic properties on hydrological process in the upper reach of the Heihe River in the Qilian Mountains, Northwest China. *Hydrological Processes* **29**: 3318–3327. DOI:10.1002/hyp.10437.
Koutsoyiannis D, Kozonis D, Manetas A. 1998. A mathematical framework for studying rainfall intensity-duration-frequency relationships. *Journal of Hydrology* **206**: 118–135. DOI:10.1016/S0022-1694(98)00097-3.
Lado M, Paz A, Ben-Hur M. 2004. Organic matter and aggregate-size interactions in saturated hydraulic conductivity. *Soil Science Society of America Journal* **68**: 234–242. DOI:10.2136/sssaj2004.2340.
Lai J, Ren L. 2007. Assessing the size dependency of measured hydraulic conductivity using double-ring infiltrometers and numerical simulation. *Soil Science Society of American Journal* **71**: 1667–1675. DOI:10.2136/sssaj2006.0227.
Li N, Wang XJ, Shi M, Yang H. 2015. Economic impacts of total water use control in the Heihe River Basin in Northwestern China – an integrated CGE-BEM modeling approach. *Sustainability* **7**: 3460–3478.
Li YY, Shao MA. 2006. Change of soil physical properties under long-term natural vegetation restoration in the Loess Plateau of China. *Journal of Arid Environments* **64**: 77–96. DOI:10.1016/j.jaridenv.2005.04.005.
Li ZL, Xu ZX, Shao QX, Yang J. 2009. Parameter estimation and uncertainty analysis of SWAT model in upper reaches of the Heihe river basin. *Hydrological Processes* **23**: 2744–2753. DOI:10.1002/hyp.7371.
Liang ZM, Zhong PA, Hua JP. 2008. Hydrology and hydrological calculation. China Water&Power Press: Beijing(in Chinese).
Lin H. 2010. Earth's critical zone and hydropedology: concepts, characteristics, and advances. *Hydrology and Earth System Sciences* **14**: 25–45. DOI:10.5194/hess-14-25-2010.
Liniger H, Weingartner R, Grosjean M. 1998. Mountains of the world: water towers for the 21st century. University of Berne: Berne, Switzerland.
Liu H, Zhao WZ, He ZB. 2013. Self-organized vegetation patterning effects on surface soil hydraulic conductivity: a case study in the Qilian Mountains, China. *Geoderma* **192**: 362–367. DOI:10.1016/j.geoderma.2012.08.008.
Mcdonnell JJ, Beven K. 2014. Debates – the future of hydrological sciences: a (common) path forward? A call to action aimed at understanding velocities, celerities and residence time distributions of the headwater hydrograph. *Water Resources Research* **50**: 5342–5350. DOI:10.1002/2013WR015141.
Mcmillan HK, Srinivasan MS. 2015. Controls and characteristics of variability in soil moisture and groundwater in a headwater catchment. *Hydrology & Earth System Sciences Discussions* **19**: 1767–1786. DOI:10.5194/hess-19-1767-2015.
Niu ZR, Hu XL, Ma ZQ, Ma ZY. 2004. Analysis on the distribution regularity of the maximum point rainfall and the storm reduction index in Gansu Province. *Hydrology* **24**: 21–25. DOI:10.3969/j.issn.1000-0852.2004.04.006(in Chinese, with English abstract).
Pan QM, Tian SL. 2001. Water resources in the Heihe river basin. The Yellow River Water Conservency Press: Zheng Zhou(in Chinese).
Price K, Jackson CR, Parker AJ. 2010. Variation of surficial soil hydraulic properties across land uses in the southern Blue Ridge Mountains, North Carolina, USA. *Journal of Hydrology* **383**: 256–268. DOI:10.1016/j.jhydrol.2009.12.041.
Rachman A, Anderson SH, Gantzer CJ, Alberts EE. 2004. Soil hydraulic properties influenced by stiff-stemmed grass hedge systems. *Soil Science Society of America Journal* **68**: 1386–1393. DOI:10.2136/sssaj2004.1386.
Santra P, Chopra U, Chakraborty D. 2008. Spatial variability of soil properties and its application in predicting surface map of hydraulic parameters in an agricultural farm. *Current Science* **95**: 937–945.
Scherrer S, Naef F. 2003. A decision scheme to indicate dominant hydrological flow processes on temperate grassland. *Hydrological Processes* **17**: 391–401. DOI:10.1002/hyp.1131.
Scholl P, Leitner D, Kammerer G, Loiskandl W, Kaul HP, Bodner G. 2014. Root induced changes of effective 1D hydraulic properties in a soil column. *Plant & Soil* **381**: 193–213. DOI:10.1007/s11104-014-2121-x.
Schwen A, Zimmersmann M, Bodner G. 2014. Vertical variations of soil hydraulic properties within two soil profiles and its relevance for soil water simulations. *Journal of Hydrology* **516**: 169–181. DOI:10.1016/j.jhydrol.2014.01.042.
Shabtai I, Shenker M, Edeto W, Warburg A, Ben-Hur M. 2014. Effects of land use on structure and hydraulic properties of Vertisols containing a sodic horizon in northern Ethiopia. *Soil and Tillage Research* **136**: 19–27. DOI:10.1016/j.still.2013.09.007.
Shi YG, Zhao XN, Gao XD, Zhang SL, Wu PT. 2015. The effects of long-term fertiliser applications on soil organic carbon and hydraulic properties of a loess soil in China: fertiliser applications impacts on SOC and hydraulic properties. *Land Degradation & Development* **27**: 60–67. DOI:10.1002/ldr.2391.
Upchurch DR, Wilding LP, Hartfield JL. 1988. Methods to evaluate spatial variability. In Reclamation of disturbed lands, Hossner LR (ed). CRC press: Boca Raton, FL; 201–229.
Vereecken H, Huisman JA, Franssen HJH, Brüggemann N, Bogena HR, Kollet S, Javaux M, Kruk JVD, Vanderborght J. 2015. Soil hydrology: recent methodological advances, challenges, and perspectives. *Water Resources Research* **51**: 2616–2633. DOI:10.1002/2014WR016852.
Viviroli D, Dürr HH, Messerli B, Meybeck M, Weingartner R. 2007. Mountains of the world, water towers for humanity: typology, mapping, and global significance. *Water Resources Research* **43**. DOI:10.1029/2006wr005653.
Wang GX, Wang YB, Li YS, Cheng HY. 2007b. Influences of alpine ecosystem responses to climatic change on soil properties on the Qinghai–Tibet Plateau, China. *Catena* **70**: 506–514. DOI:10.1016/j.catena.2007.01.001.
Wang JB, Ju JT. 2007a. Comparison of lake sediment grain size results measured by two laser diffraction particle size analyzers. *Journal of Lake Sciences* **19**: 509–515. DOI:10.18307/2007.0503(in Chinese, with English abstract).
Wang TJ, Zlotnik VA, Wedin D, Wally KD. 2008. Spatial trends in saturated hydraulic conductivity of vegetated dunes in the Nebraska Sand Hills: effects of depth and topography. *Journal of Hydrology* **349**: 88–97. DOI:10.1016/j.jhydrol.2007.10.027.
Wang YQ, Shao MA, Liu ZP. 2012. Pedotransfer functions for predicting soil hydraulic properties of the Chinese Loess Plateau. *Soil Science* **177**: 424–432. DOI:10.1097/SS.0b013e318255a449.
Wang YQ, Shao MA, Liu ZP. 2013a. Vertical distribution and influencing factors of soil water content within 21-m profile on the Chinese Loess Plateau. *Geoderma* **193-194**: 300–310. DOI:10.1016/j.geoderma.2012.10.011.
Wang YQ, Shao MA, Liu ZP, Horton R. 2013b. Regional-scale variation and distribution patterns of soil saturated hydraulic conductivities in surface and subsurface layers in the loessial soils of China. *Journal of Hydrology* **487**: 13–23. DOI:10.1016/j.jhydrol.2013.02.006.
Wilding LP. 1985. Spatial variability: its documentation, accommodation and implication to soil survey. In Soil spatial variability, Nielsen DR, Bouma J (eds). Pudoc: Wageningen; 166–194.
Wu ZL, Jia WX, Liu YR, Zhang YS. 2014. Change of vegetation coverage in the Qilian Mountains in recent 10 years. *Arid Zone Research* **31**: 80–87. DOI:10.13866/j.azr.2014.01.023(in Chinese, with English abstract).
Yang J, Nie Y, Chen H, Wang S, Wang K. 2016. Hydraulic properties of karst fractures filled with soils and regolith materials: implication for their ecohydrological functions. *Geoderma* **276**: 93–101. DOI:10.1016/j.geoderma.2016.04.024.
Yao SX, Zhang TH, Zhao CC, Liu XP. 2013. Saturated hydraulic conductivity of soils in the Horqin Sand Land of Inner Mongolia, northern China. *Environmental monitoring and assessment* **185**: 6013–6021. DOI:10.1007/s10661-012-3002-5.
Yi YL. 2009. Study on soil physics methods. Peiking University Press: Beijing, China; 147–149(in Chinese).
Yin ZL, Xiao HL, Zou SB, Zhu R, Lu ZX, Lan YC, Shen YP. 2014. Simulation of hydrological processes of mountainous watersheds in inland river basins: taking the Heihe Mainstream River as an example. *Journal of Arid Land* **6**: 16–26. DOI:10.1007/s40333-013-0197-4.
Zeng C, Zhang F, Wang QJ, Chen YY, Joswiak DR. 2013. Impact of Alpine meadow degradation on soil hydraulic properties over the Qinghai–Tibetan Plateau. *Journal of Hydrology* **478**: 148–156. DOI:10.1016/j.jhydrol.2012.11.058.
Zhang F, An Y. 2016. Vegetation greenness response to water availability in northern China from 1982 to 2006. *Solid Earth* **7**: 995–1002. DOI:10.5194/se-7-995-2016.
Zhang H, Wen YL, Li MA, Chang ZQ, Wang JY. 2001. The Climate features and regionalization of vertical climatic zones in the northern slope of Qilian Mountains. *Journal of Mountain Research* **19**: 497–502. DOI:10.3969/j.issn.1008-2786.2001.06.003(in Chinese, with English abstract).

Zhang H, Zhang B, Zhao CY. 2011. Annual base flow change and its causes in the upper reaches of Heihe River. *Geographical Research* **30**: 1421–1430(in Chinese, with English abstract).

Zhang LH, Jin X, He CS, Zhang BQ, Zhang XF, Li JL, Zhao C, Tian J, Demarchi C. 2016. Comparison of SWAT and DLBRM for hydrological modeling of a mountainous watershed in arid Northwest China. *Journal of Hydrologic Engineering* : 21. DOI:10.1061/(ASCE)HE.1943-5584.0001313.

Zhao XN, Wu PT, Gao XD, Tian L, Li HC. 2014. Changes of soil hydraulic properties under early-stage natural vegetation recovering on the Loess Plateau of China. *Catena* **113**: 386–391. DOI:10.1016/j.catena.2013.08.023.

Zhao XN, Wu PT, Gao XD, Persaud N. 2015. Soil quality indicators in relation to land use and topography in a small catchment on the Loess Plateau of China. *Land Degradation & Development* **26**: 54–61. DOI:10.1002/ldr.2199.

Zimmermann B, Elsenbeer H. 2008. Spatial and temporal variability of soil saturated hydraulic conductivity in gradients of disturbance. *Journal of Hydrology* **361**: 78–95. DOI:10.1016/j.jhydrol.2008.07.027.

Zimmermann B, Elsenbeer H. 2009. The near-surface hydrological consequences of disturbance and recovery: a simulation study. *Journal of Hydrology* **364**: 115–127. DOI:10.1016/j.jhydrol.2008.10.016.

Zimmermann B, Elsenbeer H, De Moraes JM. 2006. The influence of land-use changes on soil hydraulic properties: implications for runoff generation. *Forest Ecology and Management* **222**: 29–38. DOI:10.1016/j.foreco.2005.10.070.

